EUROGRAPHICS Workshop on Graphics and Cultural Heritage (2014)
R. Klein and P. Santos (Editors)

Similarity assessment for the analysis of 3D artefacts

S. Biasotti[1], A. Cerri[1], B. Falcidieno[1], M. Spagnuolo[1]

[1]Istituto di Matematica Applicata e Tecnologie Informatiche "E. Magenes", CNR, Italy

Abstract

Archaeological artefacts are often classified in homogeneous groups, with respect to their origin, use, age, etc., in terms of their physical traits, i.e., colour, material, design pattern, form, shape, size, style, surface texture, technology, thickness, and weight. In particular, when dealing with archaeological exhibits, a single trait is generally not enough for the classification of the artefact because most of the objects are affected by degradation or only partially preserved. In this contribution we propose a shape analysis and comparison pipeline, which combines geometry and texture to identify classes of homogeneous artefacts. The geometric description is based on a statistical technique to select properties that are mutually independent; the photometric information is handled according to a topological perspective, and complemented by the analysis of colour distribution. The outcome is a mixed description of each 3D artefact, which is used to derive a similarity measure between objects. The potential of our method is high since we can include any property representable as real- or vector-valued functions. Experimental results are exhibited to show the efficacy of the method in retrieval and classification tasks.

Categories and Subject Descriptors (according to ACM CCS): Computer Graphics [I.3.6]: Methodology and Techniques—Information storage and retrieval [H.3.3]: Information search and Retrieval—

1. Introduction

Reconstructing and analysing 3D digital environments has been a factor of success in many industrial, social, and entertainment contexts. Also in the Cultural Heritage (CH) environment, it is now becoming a powerful communication and interaction tool and an effective and efficient means to learn, access information, organize and structure knowledge.

In the last years, numerous and various initiatives contributed to the development of methods, tools and technologies for the creation of digital libraries for CH embedding different media [Arn14]. Various aspects and technological advancements help to make the world's cultural heritage available on line. First of all the increasing performance and proliferation of 3D scanning devices and digital photography has made it possible to acquire at reasonable costs very dense and accurate sampling of both geometric and visual properties of real objects. A variety of digital libraries for archaeology have been developed and supported (see, e.g., http://www.daacs.org/ or http://sites.matrix.msu.edu/dakar/). In particular, it is worth to mention EUROPEANA (http://www.europeana.eu/), a platform for collecting European CH and for enabling searching and exploring heritage across several European cultural institutions. These large efforts focus on the gathering of the information and on providing a wide range of source materials to as large an audience as possible.

The recent EU report 'New Renaissance' [NDL11] recommends that *"cultural institutions should make public domain material digitised with public funding as widely available as possible for access and re-use"*. The wider and wider availability of sampled 3D models is predicted to have the impact of photography at the end of 19th century.

To realize this vision, we cannot focus only on the improvements of the acquisition and visualization processes. Despite a general agreement on the potential of visualization in disseminating knowledge of cultural heritage, the new challenge lies in developing specific applications to assist users (scientists, scholars, curators, restorers, common citizens,..) to model, retrieve, compare, analyse, document, classify, catalogue artwork.

Over the past 5 to 10 years, a number of initiatives and projects have positively influenced the scientific community in order to develop new 3D intelligent content creation and processing tools. Examples include AIM@SHAPE [IST08], FOCUS K3D [IST10], 3D-COFORM [IST12], V-Must [IST15]. Due to these actions, in the creation of cul-

DOI: 10.2312/gch.20141313

tural heritage digital content, we are assisting to a continuous progress in digital acquisition tools [Sin14].

To exploit these new technologies, new software tools are required (3DCH is more than acquisition and visualization!). For example one of the most common and critical activities that CH researchers, anthropologists and museum curators perform is to carry out comparisons of artefacts within and across collections and institutions. Comparative analysis is a core step in the methodology for classifying and curating artwork, it also enables historians to track changes in techniques, tools or materials that were associated with the production, decoration, or use of an artefact. What is crucial is to provide archaeological researchers mechanisms to compare objects and fragments, identify patterns and textures, examine material properties, filter noise and degradation effects on the remains, take advantage of all data and knowledge acquired to appropriately cluster similar parts.

What are the challenges that make content-based retrieval or classification even more complex in the CH field? Archaeological artefacts are often broken, eroded, worn, or incomplete, their quantity is extremely vast, distributed and fragmented, and there is an intrinsic uncertainty of what data represent and in the variety of possible valid descriptions. The nature of CH data calls for methods dealing with multi-modal information in combination (e.g., texture and reflectance), which is necessary to effectively group artefacts or their parts into meaningful clusters. This is actually in contrast with the current scenario: most of the state-of-the-art methodologies for matching or retrieving similar objects in repositories are based on the analysis of single geometric properties of the object shape.

In this paper we propose a shape analysis and comparison pipeline specifically targeted to the similarity assessment of *real-world* 3D artefacts. The proposed methodology takes the above needs into account being able to concurrently evaluate heterogeneous properties, such as geometric (eg, curvature, size, roundness or mass distribution) and photometric aspects (e.g., texture, colour distribution or reflectance). Indeed, since object variability is high and assets may possibly be cracked or incomplete, it is important to rely on a large number of descriptors: this will allow for the construction of signatures that may take into account properties of interest for users that are difficult to characterize in a precise manner. Additionally, our method relies on a tuning phase where the descriptors themselves are selected and used in the final configuration according to their performance in characterizing objects according to the user needs. In our framework, we can include any property, which can be defined by real or vector-valued functions defined on the assets boundary.

Our approach takes inspiration from that proposed in [BCGS13], in the sense of combining a description based on geometric functions with a topological analysis of photometric properties. However, the specificity of the application domain and the real-world nature of the analyzed models open new perspectives and call for a reformulation of these ideas, in order to solve additional problems such as material and colour deterioration, illumination changes, etc. In particular, texture analysis has been refined by introducing an additional photometric description based on colour histograms, and a different technique for the selection of the most informative geometric properties has been considered.

The remainder of the paper is organized as follows. In Section 2, we introduce the related previous work, Section 3 defines our method and describes how to handle geometric and photometric information. Experimental results are shown and commented in Section 4 and some conclusive remarks are outlined in Section 5.

2. Previous work

While the combination of shape and colour information is quite popular in image retrieval [GS00] and processing [KMS00, LJ05], the attention towards texture properties for 3D shape analysis has considerably grown only in the last few years, as also demonstrated by the proposal of dedicated benchmarks to evaluate their retrieval and classification performances [CBA*13, BCA*14].

Among the first attempts to devise 3D descriptors that combine geometric and photometric information, Suzuki et al. [Suz01] used colour information represented as the Phong's model parameters to complement the retrieval process. Colour and 3D shape information are used to build a concatenated surface descriptor [SH07] or to combine geometric similarity based on Shape Distributions [OFCD02] with colour similarity computed through the comparison of colour distribution histograms [RCMH09]. All these methods consider colour as a general property and its spatial distribution over the shape is not considered.

To generalize image-based descriptors, [WCL*08] proposed VIP, a SIFT-based descriptor using 3D oriented patches, whereas [CO06, PZC13] introduced Textured Spin-Images, an extension of classical Spin Images to meshes whose vertices have luminance information. Kanezaki et al. [KHK10] proposed colour-CHLAC Features computed on 3D voxel data: each voxel has a 6-dimensional status describing both occupation and RGB colour information, so that local descriptors can be represented by the co-occurrence of their shape and texture patterns. Liu et colleagues [LZL*12] proposed a sampling method that picks points in regions of either geometry-high variation or colour-high variation, and define a signature based on feature vectors computed at these points. Tombari et al. [TSDS11] introduced the CSHOT descriptor, meant to solve the surface matching problem based on local features, i.e. by point-to-point correspondences obtained by matching shape- and colour-based local invariant descriptors of feature points.

Recently, attention has been paid to invariant shape properties of deformable or articulated 3D objects. An exam-

ple is meshHOG, a geometric SIFT-like descriptor for textured shapes directly defined on the surface [ZBH12]. Such a method builds upon a scale-space derived from different normalized Gaussian derivatives through the Difference-of-Gaussians (DoG) operator [Low04], and incorporates in a unique paradigm geometry and photometric information. The operator is computed on a scalar function defined on the manifold, which is either the mean curvature, the Gaussian curvature or the photometric appearance of a vertex (the mean of the RGB channels). A local descriptor, called MeshHOG, is obtained as a two-level histogram of the projections of the gradient vectors onto the three orthogonal planes associated with the local coordinate systems of the maxima and minima of the scale space representation. To have invariance to the mesh sampling, the concatenated histograms are normalized through the L_2-norm, that is also used to compare two meshHOGs. Similarly, the Photometric Heat Kernel Signatures (PhotoHKS) [KBBK12, KBB*12, KRB*13] use the diffusion framework to embed the shape into a high-dimensional space where the embedding coordinates represent the photometric information. In practice, the method fuses geometry and photometry in a local-global description that generalizes Heat Kernels and Shape Distributions [OFCD02]. Following the same intuition, in [BCGS13] the geodesic distance is generalized to a hybrid shape description able to couple geometry and texture.

3. Shape description and comparison combining geometry and photometry

Our method relies on the paradigm that the shape similarity among objects may be assessed in terms of representative features, along with their relationships and their invariants. We further assume that such shape properties can be described by scalar- or vector-valued functions defined on suitable discrete representations of the objects (e.g., triangle meshes) [FS98]. Based on this, recent advances in topological methods for the analysis of functions [CL13], and the introduction of learning techniques to group and select functions [BSF13, BB13, BB14] set the theoretical foundations of our approach. Working this way has a twofold benefit: on the one hand, the topological description is characterized by a rigorous notion of stability against function perturbations, which implies robustness to noise in concrete applications. On the other hand, learning techniques can be used to select functions, that is features, that better describe objects in a given application scenario. The combination of the two provides a flexible and modular way to incorporate in the same framework multiple, heterogeneous properties and invariants and make them fitting the specific domain to be analysed.

More specifically, to automatically identify geometric properties that are mutually independent, as well as to select the most salient ones, we cluster a collection of scalar functions that represent such properties using the approach defined in [BSF13], see Section 3.1. This allows us to consider from the very beginning a large number of shape properties, which is indeed particularly helpful here, since the variability of information is possibly increased by the fact that artefacts might be affected by cracks or missing parts.

To study photometric properties of the archaeological artefacts, we represent colour as real- and vector-valued functions defined in the CIELab space, and analyse such functions from a topological perspective using *persistence* [CL13]. In this way we get additional, structured information that complements the traditional analysis based on colour histograms. Details on these descriptions are provided in Sections 3.2.1 and 3.2.2.

The geometric and photometric descriptions associated with different shapes are then compared through suitable metrics to derive as many distances; these are further combined into a final score for shape similarity assessment. We detail this procedure in Section 4.2.

3.1. Geometric description

To represent the geometric properties of shapes, we considered a set of 70 functions reflecting either intrinsic or extrinsic shape features. Functions encoding the distance from significant points highlight the distribution of the object with respect to those points; distances from the main shape axis or the associated orthogonal planes characterize the invariance with respect to axis rotations and symmetries; curvature-, geodesic- and Laplacian-based functions are pose invariant because they approximate the intrinsic Riemannian metric of the surface [BBK06]; a complete list of functions and discussions on their properties can be found in [BSF13]. These scalar functions play the role of the vocabulary of invariants and properties used to code a shape.

Figure 1 displays some functions we considered in our setting; namely, the Fiedler vector $1(a)$, the Gaussian and the Mean curvature $1(b,c)$, the distance from the center of mass $1(d)$, the average of the geodesic distances $1(e)$, two different mixes of Laplacian eigenfunctions $1(f,g)$, a Heat kernel function $1(h)$, the distances along the principal shape axis $1(i)$ and the symmetry plane $1(j)$, the orthogonal distance from the main shape axis $1(k)$ and the symmetry plane $1(l)$. Even in case of "few" functions as in Figure 1, we notice how their evolution over the shape is sometimes qualitatively similar and probably redundant, see for instance Figures $1(a,j)$ and $1(d,e,h)$, or the difference is mainly on the sign of the function, see Figures $1(a,h)$ and $1(g,l)$.

Therefore, we aim at selecting the most significant functions, possibly keeping as much information as possible. The selection of functions can be easily adapted to the dataset: depending on the shape variability or the characteristics of the objects in a repository the choice of the functions might change even if the same framework is still valid.

In this scenario, we adopt the grouping approach proposed

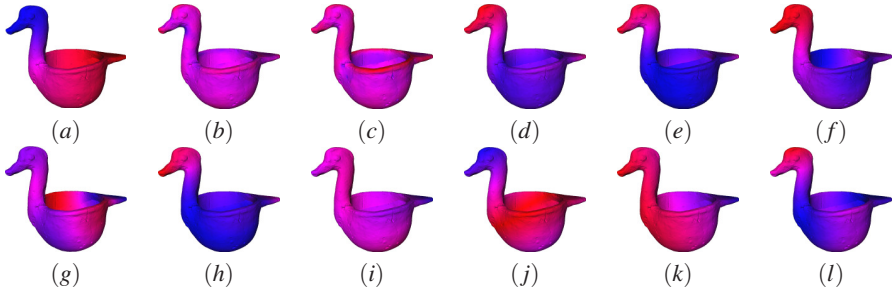

Figure 1: *A set of the functions considered in our framework. Colours represent the function from low (blue) to high (red) values.*

in [BSF13] to select a subset $F' \subseteq F$ of scalar functions that qualitatively preserve the descriptive power of the original set F. The method groups the functions according to a distance defined on F in a completely unsupervised manner and for each shape class it is possible to identify a (small) number of functions that are mutually independent.

Given a set $F = \{f_1, \ldots, f_n\}$ of n functions defined on a triangle mesh T representing a shape, the distance $\mathcal{I}(f_i, f_j)$ for $f_i, f_j \in F$ is defined as:

$$\mathcal{I}(f_i, f_j) := \frac{1}{\text{area}(T)} \sum_{t \in T} \left| < \frac{\nabla^t f_i}{\|\nabla^t f_i\|}, \frac{\nabla^t f_j}{\|\nabla^t f_j\|} > \right|,$$

with $\nabla^t f_i$, $\nabla^t f_j$ representing the gradient of f_i and f_j over the triangle t. Intuitively, we are assuming that a relevant discrepancy in the distribution of the gradients of two functions f_i and f_j implies that they are significantly different.

A *mutual distance matrix MDM* with entries $MDM_{ij} := 1 - \mathcal{I}(f_i, f_j)$ is used to store the distances between all the possible couples of functions. Indeed, the ith row (or column) of the matrix identifies all the distances of f_i with respect to $f_1, \ldots, f_n$, and (partially) orders the distances between f_i and the others in F. The minima of the ith row correspond to functions that are qualitatively similar to f_i, while maxima highlight functions that significantly differ.

Based on these premises, we aim at grouping the elements of F in such a way that the functions within the same group (cluster) have a high internal homogeneity, while they are strongly dissimilar from the entities of a different cluster. According to [PP07], we represent a cluster as an n-dimensional vector $x = (x_i)$, whose components are real numbers expressing the level of participation of functions in the cluster. A small value for x_i means that the corresponding function f_i is weakly associated to the cluster, whereas a high value means that the function is strongly associated to it. Components corresponding to functions not participating in the cluster are zero. The cohesiveness of the elements of a cluster is expressed in terms of the quadratic form $Q = x^T MDM\, x$ so that the (pairwise) clustering problem is reduced to that of finding a vector x maximizing Q.

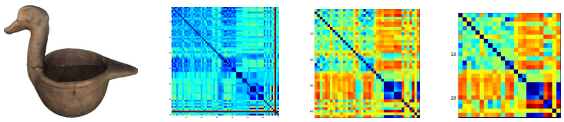

Figure 2: (a) *A model from the dataset and* $(b-d)$ *the corresponding MDM signature with 70, 42 and 22 functions. The distances range from blue (zero) to red (1); large blue regions indicate functions that are strongly similar.*

In practice the clustering problem is solved by the following quadratic program (see the formal proof in [PP07]):

$$\text{maximize } x^T MDM\, x,\ x \in \Delta^n, \tag{1}$$

where Δ^n is the standard simplex of $\mathbb{R}^n$. We locally solved Eq. (1) via the so-called *replicator dynamics technique* [Wei95], which iteratively identifies a cluster by finding a local solution of Eq. (1), and removes the corresponding rows and columns from the matrix MDM. This technique can be summarized in the following three steps:

1. find a local solution of Eq. (1) selecting the components of x such that $x_i \geq \varepsilon$, here ε is a *cohesiveness* threshold fixed by the user;
2. remove the functions already clustered by deleting the corresponding rows and columns in the matrix MDM;
3. reiterate on the remaining functions.

In this way, a smaller number of functions is selected out of the starting ones, each one being a representative of a cluster. For each model S in the dataset, these functions have been used to compute a reduced version of $MDM(S)$. Figure 2 shows an example of the MDM signature of a 3D object with respect to 70 functions and its reduced version with 42 and 22 functions.

3.2. Photometric description

Photometric properties can be represented in different colour spaces, such as the RGB and HSV spaces. We opt here for

the CIELab one [Fai05]. Defining measures in the CIELab colour space is justified by physiological studies, showing that it well represents how the human eye perceives colours. Moreover, in the CIELab space tones and colours are held separately: the L channel is used to specify the luminosity or the black and white tones, whereas the a channel specifies the colour as either a green or a magenta hue and the b channel specifies the colour as either a blue or a yellow hue.

We consider two ways to deal with the photometric information: the persistence framework (Section 3.2.1) and colour histograms (Section 3.2.2).

3.2.1. Persistence diagrams and spaces

To include the CIELab coordinates in the persistence framework we follow the approach adopted in [BCGS13]. We consider the a, b channels as jointly defining a bivariate function over a given shape, whereas L is used separately as a scalar function. In this way, colour and intensity are treated separately. More precisely, for a shape S we consider two functions $f_L : S \to \mathbb{R}$ and $f_{a,b} : S \to \mathbb{R}^2$, the former taking each point $p \in S$ to the L-channel value at p, the latter to the pair given by the a- and the b-channel values at p, respectively. The values of f_L and $f_{a,b}$ are normalized to range in [0,1]. Similarly to [BCGS13], we consider the $0th$ persistence diagram of f_L and the $0th$ persistence space of $f_{a,b}$.

Roughly speaking, the $0th$ persistence diagram of f_L associated with S encodes the topological evolution of S by counting the number of connected components which remain disconnected passing from a lower level set S_u of S to another lower level set S_v with $u < v$, where a lower level set is defined as $S_u = \{p \in S : f_L(P) \leq u\}$, for $u \in \mathbb{R}$. As shown by Figure 3, a persistence diagram can be seen as a collection of points lying in the half-plane $\{(u,v) \in \mathbb{R}^2 : u < v\}$, (red dots in Figure 3$(c,d)$). Each point (u,v) in the diagram describes the *lifespan* of a connected component: the u-coordinate denotes the value of f_L at which a new component appears in the associated lower level set S_u; similarly, the v-coordinate denotes the value of f_L at which that component merges with an existing one. The distance from the diagonal $u = v$ represents the component lifespan, which in turn mirrors the importance of the feature that component represents: points far from the diagonal describe important, long-lived features, whereas points close to the diagonal describe local information such as smaller details and noise. The red vertical line in Fig 3(a), as well as the one in Fig 3(b), can be seen as a point at infinity, representing a connected component that will never die, i.e. its u-component corresponds to the smallest value for f_L on S, and its v-component is equal to $+\infty$. Persistence diagrams are stable shape descriptors: small changes in the function f_L induces only small changes in the corresponding diagrams [CSEH07]. An intuition of this is given by Figure 3(c,d): the two models have similar luminosity, resulting in similar configurations for the points far from the diagonal in the associated persistence diagrams og f_L.

In the context of persistence, the use of vector-valued functions leads to a generalization of the notion of persistence diagram to that of *persistence space* [CL13]. For each shape S, we consider here the $0th$ persistence space associated with the bivariate function $f_{a,b}$ defined on S. Unfortunately, the persistence spaces of a bivariate function are sets of continuous structures living in $\mathbb{R}^4$. Being continuous, this implies that concretely we can only get approximations of a $0th$ persistence space of $f_{a,b}$. Following [BCGS13], this can be done by considering a collection of suitable $0th$ persistence diagrams computed as follows:

1. let P be the set points in the triangle mesh representing a shape S, and let M be the greatest value between $\max_{p\in P} a(p)$ and $\max_{p\in P} b(p)$;
2. being k the cardinality of P, fix $\log k$ equally distributed real values i in the interval $(0,1)$, and as many equally distributed real values j in the interval $[-M,M]$;
3. for every i and j, compute the $0th$ persistence diagram for the function $F_{ij} : P \to \mathbb{R}$ taking each $p \in P$ to
$$F_{ij}(p) = \max\left\{\frac{a(p)-j}{i}, \frac{b(p)+j}{1-i}\right\};$$
4. for every point (u,v) in the $0th$ persistence diagram of F_{ij}, project it back to a point $(u_1,u_2,v_1,v_2) \in \mathbb{R}^4$ through the equations
$$(u_1,u_2) = (i,1-i)u + (j,-j);$$
$$(v_1,v_2) = (i,1-i)v + (j,-j).$$

The set of all points in $\mathbb{R}^4$ obtained according to the above procedure gives us an approximation for the $0th$ persistence space of $f_{a,b}$: its stability as a shape descriptor follows directly from that of the $0th$ persistence diagrams for F_{ij} [CL13]. For the practical computation of persistence diagrams (which is directly connected with the approximated computation of persistence spaces) we refer to [EH10].

We remark that, while analysing the purely photometric information related to the distribution of *Lab* colour channels, the topological approach also takes into account the connectivity of the underlying model, as persistent diagrams and spaces are computed by sweeping the sub-level sets induced on the shape model by the considered functions.

3.2.2. Colour histograms

The stability properties of persistence diagrams and spaces imply resistance to noise when it comes in the form of small perturbations in the L, a, b values. In particular, the topological approach ensure robustness even when the small changing in the CIELab colour coordinates are widely spread over the shape model. In practical situations, this may happen when material degradation results in large spots affecting the surface artefact, see e.g. Figure 5(l).

However, the proposed approach is not optimal when photometric noise is given by large variations in the L, a, b values, even when such variations are confined in small por-

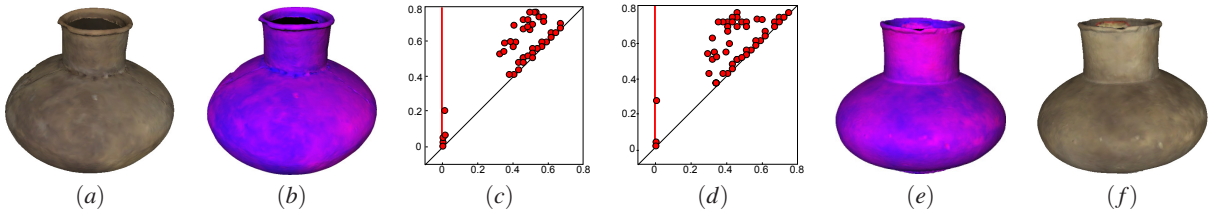

Figure 3: *A model in the dataset (a), the corresponding L channel ((b), colour coded from blue for low values to red for hight values) and the 0th persistence diagram of f_L (c). Analogously in (f), (e) and (d), respectively, for a different model.*

tions of a surface model. For example, this could be the case of cracks occurring on the surface artefact, possibly resulting in threadlike structures characterized by a sudden colour variation, see e.g. Figure 5(*m*).

For this reason, we complement the persistence-based description with a purely photometric contribution based on colour histograms. Indeed, these colourimetric descriptors behave well against localized noise, since it does not alter colour distribution too much. Each considered shape is then associated with a colour histogram given by the concatenation of the three colour channels (*Lab*).

4. Experimental results

The proposed shape descriptions have been adopted on a collection of artefacts represented as textured triangle meshes, an tested in a retrieval and classification scenario with promising results. The combination of geometric and photometric properties allows us to have good performances in detecting artefacts sharing visually similar texture, even if models are either affected by noise, such as colour and pattern degradation, or characterized by missing parts.

4.1. The Dataset

Experiments are carried on the collection of textured 3D triangle meshes provided by the Virtual Hampson Museum (VHM, http://hampson.cast.uark.edu), see Figure 4. The dataset comprises 442 models, 395 of them available for download, representing as many American Indian artefacts largely produced from 350 to 600 years ago. Most of models are grouped into three geometric classes, namely bottles (189 elements), bowls (112 elements), and jars (73 elements). However smaller ones have also been detected by VHM experts, for a total amount of 12 geometric classes.

No texture classification of the dataset is provided and some models do not have any texture. However, several objects represented in the dataset are made up of the same material, such as ceramic or stone, or are characterized by similar decorations, namely paintings or relief ornaments. All these properties can be expressed in terms of photometric information, which is in turn handled as *Lab* information equipping the purely geometric 3D models. Figure 5 shows some examples of the models; we highlight that some objects share both geometry and texture (e.g. models 5(*a*,*b*) and 5(*l*,*m*)) while in some cases the geometric similarity is only partial (e.g. models 5(*g*,*h*) and 5(*l*,*n*)).

4.2. The final signature and similarity assessment

For each triangle mesh we consider the geometric and the photometric descriptions detailed in Section 3. In particular, the geometric distance $d_G(S_1,S_2)$ between two shapes S_1 and S_2 is computed as the Manahattan distance [DD09] between the associated matrices $MDM(S_1)$ and $MDM(S_2)$; the photometric distance based on persistence $d_P(S_1,S_2)$ is the normalized sum of the Hausdorff distance between the $0th$ persistence diagrams of f_L and that between the $0th$ persistence spaces of $f_{a,b}$, respectively; the purely photometric distance $d_H(S_1,S_2)$ is the L_1-norm between the concatenated colour histograms. Then, the combined distance $D(S_1,S_2)$ between S_1 and S_2 is defined as:

$$D(S_1,S_2) = \lambda_1 d_G(S_1,S_2) + \lambda_2 d_P(S_1,S_2) + \lambda_3 d_H(S_1,S_2),$$

where $0 \leq \lambda_1,\lambda_2,\lambda_3 \leq 1$, $\lambda_1+\lambda_2+\lambda_3 = 1$ and $d_G(S_1,S_2)$, $d_P(S_1,S_2)$, $d_H(S_1,S_2)$ are beforehand normalized to range in the interval [0,1].

For most of the experiments proposed here, we opted for a *balanced* combination of geometric and photometric information, i.e. $\lambda_1 = \lambda_2 = \lambda_3$. Indeed, the contribution of d_G is purely geometric, d_H is purely photometric and d_P is photometric as well, yet taking into account the connectivity of the underlying model. Note however, that any other weighted combination for the three contributions could be used, thus adapting the machinery to specific comparison, retrieval or classification tasks, see discussions in Section 4.3.

4.3. Examples

Figures 6, 7, 8, 9 show some retrieval results. In all figures, each row corresponds to a retrieval example. In the examples, models are ordered from left to right; the first column is the query model, it is always the first retrieved item and hence it is never repeated; shaded images represents correct retrievals according to the geometric dataset classification.

Figure 6 provides four examples of how the balanced

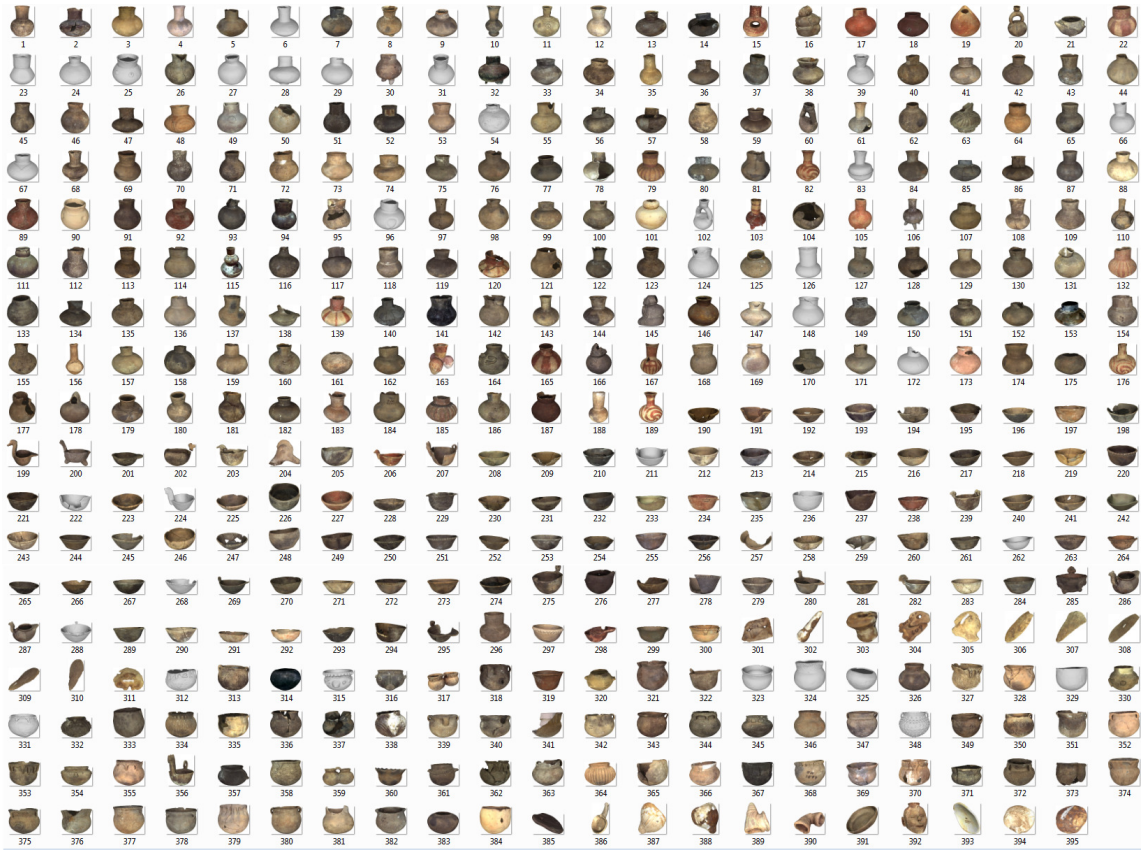

Figure 4: *The Virtual Hampson Museum dataset.*

combination of geometric and photometric information works in our settings, when looking for objects in the dataset that are similar to a hoe (first row), a bowl (second and third row) and a jar (last row). On the one hand, our method seems to be able to detect similar geometric shapes even in the presence of small holes (second and fourth row) or missing parts (third row) in the query model. On the other hand, the retrieved items exhibit similar photometric properties, even in case of noise and degradation effects.

Figure 5: *Samples from the dataset: models $(a-f)$ (resp. $(g-i)$ and $(l-n)$) belong to the same geometric class, also showing similar textures.*

Figure 6: *Retrieval examples: searching for models similar to a hoe (first row), a bowl (second,third row), and a jar (fourth row).*

Figure 7 highlights the ability of the proposed method in dealing with texture information. The first row shows the

potential of our technique in detecting similar patterns and colour distributions; the second and third examples highlight that it is also possible to cluster models made up of the same material. It is worth mentioning that our method works fine in the presence of noise, when it comes in the form of either pattern degradation (first row, fifth column) or changing in the lighting conditions (first row, second column; second row, third and fifth column). Also, our approach appears to be insensitive to photometric perturbations due to either material deterioration (second row, second and fourth column) or the presence of colour spots (second row, third column; last row, last column), or even caused by cracks on the surface model (second row, first and fourth column; last row, first and second column).

Figure 7: *Retrieving objects with similar decorative pattern/colour distribution (first row), or made up with the same material (resulting in similar textures, last two rows).*

Tuning weights. In general, the retrieval and classification effectiveness largely depends on the data and the query submitted. For example, trying to properly classify a fragment of an artefact, we would probably take into large account information about material and decorative patterns. On the contrary, geometric properties of the fragment might not be extremely relevant, since probably they do not reveal useful insight about the geometric aspect of the original artefact. Motivated by these remarks, we may consider also different choices of $\lambda_1, \lambda_2, \lambda_3$. In concrete applications, the weights λ_i can be determined either statistically a priori, or dynamically refined according to the data. Figure 8 shows an example about augmenting λ_1 by a factor 2.5 (second row) with respect to the balanced combination given by $\lambda_1 = \lambda_2 = \lambda_3$ (first row). As can be seen, tuning the combination of geometric and photometric contributions according to different weights can greatly improve the geometric retrieval performance.

Quite conversely, in the example in Figure 9, λ_1 has been reduced by a factor 4 (second row). As shown in the pictures, as soon as the photometric properties are taken in larger account, reddish objects appear earlier in the retrieval list. At the same time, the geometric retrieval performance decreases, indeed a reddish bottle is now in the top five retrieved items.

Figure 8: *By emphasizing the contribution of the geometric description (second row), we get better geometric retrieval performances.*

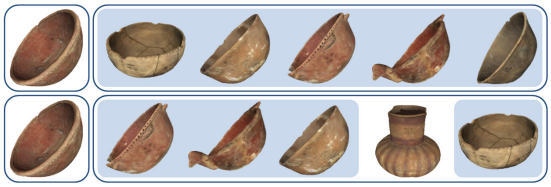

Figure 9: *By reducing the geometric contribution (second row), it is possible to increase the photometric retrieval performances.*

4.4. Retrieval and classification performance

In this section we provide a more general overview on the retrieval and classification performance exhibited by the proposed method. We remark that this evaluation is only possible at a geometric level, since the 3D model collection considered in our experiments is not provided with a ground-truth based on photometric shape properties.

Figure 10 shows the averaged precision-recall curves [BYRN99] computed according to the dataset classification provided by VHM experts, with respect to different choices of the cohesiveness threshold ε (cf. Section 3.1). Each choice of ε induces a different number of representative functions, in this example we show the performance when 42, 26, 18 and 12 functions are selected. Additionally, we compare our geometric descriptions with the well-established one based on spherical harmonics [KFR03].

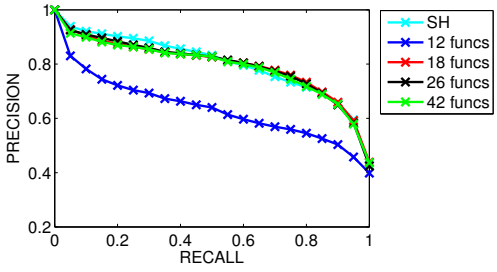

Figure 10: *Precision-recall curves for multiple instances of the proposed geometric description, in comparison with spherical harmonics.*

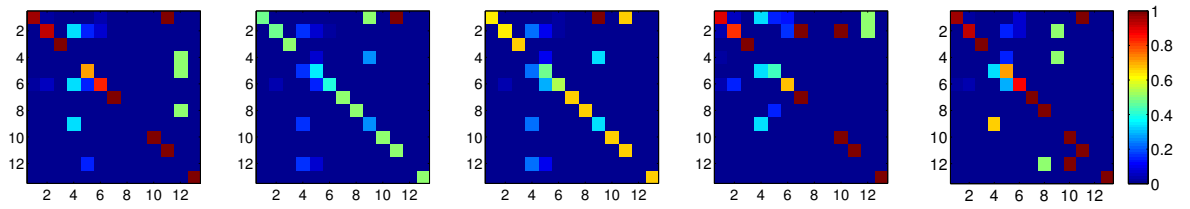

Figure 11: *Confusion matrices of the methods. From left to right: the matrices obtained with 42, 26, 18, 12 functions and the spherical harmonics, respectively.*

In a precision-recall plot, the larger the area below the curve, the better the retrieval performance. Figure 10 highlights that the performance of the method is quite stable and able to recover the geometry of the considered 3D artefacts in a way that is comparable to the spherical harmonics technique and degrades only when 12 functions or less are considered. Looking at the details of the functions that are necessary to have a good performance, we notice that performance mainly degrades when the contribution of rigid-invariant functions (such as mean curvature, distance from points and symmetry planes) is discarded from the geometric description. This is not surprising because the dataset is largely made of models that are well characterized by curvatures and spatial distributions.

The classification rate is computed using the nearest-neighbor classifier over the VHM dataset classification, and is approximately 91% for the spherical harmonics descriptor and for each run of our method, except for the description obtained with 12 functions that degrades to 82%. Finally, Figure 11 represents the confusion matrices of the different methods. For visual purposes we have normalized the matrices with respect to the number of elements in each class. Similarly to the retrieval case, we notice that the classification is quite stable and mainly fails when the classification of an object depends on its functionality rather than its geometry, see for instance class 12 (classified as *shells*) that is never correctly identified and corresponds to models 393 and 394 (second-last and third-last items) in Figure 5.

5. Conclusive remarks

In cultural heritage, 3D shapes act as a fundamental marker of trends – stylistic, geographic, historic, ethnographic. Understanding and explaining, among scientists and beyond, dependencies between these trends, as well as their evolution over time, therefore requires the introduction of tools and formalisms fostering rigorous analyses of how shapes vary across territories and periods. This variability of shapes can only be portrayed and studied if a classification effort is carried out in order to read geometric similarities, patterns, exceptions and semantics.

In this contribution we have shown how geometry and texture can be jointly combined to fruitfully support comparison of archaeological artefacts and assist the expert in the object classification. Indeed, our framework can be easily tuned to other datasets: in that case the selection of geometric functions will reflect the nature of the new collection and also the contribution of the photometric description might change to reflect different user's needs. We also highlight that the method is not limited to geometric and photometric information: indeed we can include and combine any property representable as real- or vector-valued functions.

As for future investigation, other interesting issues we see concern the inclusion of the user needs in the acquisition phase, the personalization of the framework with a user profiling strategy, the contribution to the definition of benchmarks and ground-truths, the interaction and the validation of the method with CH experts to identify how to balance the combination of several descriptors (as well as of several possible parameterizations) according to the problem at hand, the inclusion of context information (e.g. the geographic and historic information) and move towards semantic classification.

Acknowledgements. The authors wish to thank Daniela Giorgi for the useful discussions on the comparison of textured 3D shapes. Work developed in the CNR research activity ICT.P10.009, and partially supported by VISIONAIR, EU project "FP7 INFRASTRUCTURES" (2011-2015).

References

[Arn14] ARNOLD D.: Computer graphics and cultural heritage: From one-way inspiration to symbiosis, Part I. *IEEE Comput. Graph. 34*, 3 (2014), 76–86. 1

[BB13] BARRA V., BIASOTTI S.: Learning kernels on extended Reeb graphs for 3D shape classification and retrieval. In *Eurographics Workshop on 3D Object Retrieval* (2013), pp. 25–32. 3

[BB14] BARRA V., BIASOTTI S.: 3D shape retrieval and classification using multiple kernel learning on extended reeb graphs. *Visual Comput.* (2014), 1–13. 3

[BBK06] BRONSTEIN A. M., BRONSTEIN M. M., KIMMEL R.: Efficient computation of isometry-invariant distances between surfaces. *SIAM J. Sci. Comput. 28*, 5 (2006), 1812–1836. 3

[BCA*14] BIASOTTI S., CERRI A., ABDELRAHMAN M., AONO

M., HAMZA A. B., EL-MELEGY M., FARAG A., GARRO V., GIACHETTI A., GIORGI D., GODIL A., LI C., LIU Y.-J., MARTONO H. Y., SANADA C., TATSUMA A., VELASCO-FORERO S., XU C.-X.: SHREC'14 Track: Retrieval and Classification on Textured 3D Models. In *Eurographics Workshop on 3D Object Retrieval* (2014), pp. 111–120. 2

[BCGS13] BIASOTTI S., CERRI A., GIORGI D., SPAGNUOLO M.: PHOG: Photometric and Geometric Functions for Textured Shape Retrieval. *Comput. Graph. Forum 32*, 5 (2013), 13–22. 2, 3, 5

[BSF13] BIASOTTI S., SPAGNUOLO M., FALCIDIENO B.: Grouping real functions defined on 3D surfaces. *Comput. Graph. 37*, 6 (2013), 608 – 619. 3, 4

[BYRN99] BAEZA-YATES R. A., RIBEIRO-NETO B.: *Modern Information Retrieval*. Addison-Wesley Longman Publishing Co., Inc., Boston, MA, USA, 1999. 8

[CBA*13] CERRI A., BIASOTTI S., ABDELRAHMAN M., ANGULO J., BERGER K., CHEVALLIER L., EL-MELEGY M. T., FARAG A. A., LEFEBVRE F., GIACHETTI A., GUERMOUD H., LIU Y.-J., VELASCO-FORERO S., VIGOUROUX J.-R., XU C.-X., ZHANG J.-B.: SHREC'13 Track: Retrieval on Textured 3D Models. In *Eurographics Workshop on 3D Object Retrieval* (2013), pp. 73–80. 2

[CL13] CERRI A., LANDI C.: The persistence space in multidimensional persistent homology. In *Discrete Geometry for Computer Imagery* (2013), vol. 7749 of *LNCS*, pp. 180–191. 3, 5

[CO06] CORTELAZZO G. M., ORIO N.: Retrieval of Colored 3D Models. In *3rd International Symposium on 3D Data Processing, Visualization and Transmission* (2006), pp. 986–993. 2

[CSEH07] COHEN-STEINER D., EDELSBRUNNER H., HARER J.: Stability of persistence diagrams. *Discr. Comput. Geom. 37*, 1 (2007), 103–120. 5

[DD09] DEZA M. M., DEZA E.: *Encyclopedia of Distances*. Springer Berlin Heidelberg, 2009. 6

[EH10] EDELSBRUNNER H., HARER J.: *Computational Topology: An Introduction*. American Mathematical Society, 2010. 5

[Fai05] FAIRCHILD M. D.: *Color Appearance Models, 2n Edition*. Wiley-IS& T, Chichester, UK, 2005. 5

[FS98] FALCIDIENO B., SPAGNUOLO M.: A shape abstraction paradigm for modeling geometry and semantics. In *Proceedings of the Computer Graphics International* (1998), IEEE Computer Society, pp. 646–656. 3

[GS00] GEVERS T., SMEULDERS A. W.: Pictoseek: combining color and shape invariant features for image retrieval. *IEEE T. Image Process. 9*, 1 (2000), 102–119. 2

[IST08] IST: FP6 Network of Excellence: AIM@SHAPE. http://www.aimatshape.net, 2004–2008. no. 506766. 1

[IST10] IST: FP7 Coordination Action: FOCUS K3D. http://www.focusk3d.eu/, 2008–2010. no. 214993. 1

[IST12] IST: FP7 Integrating Project: 3DCOFORM. http://www.3d-coform.eu/, 2008–2012. no. 231809. 1

[IST15] IST: FP7 Network of Excellence: V-MUST. http://www.v-must.net, 2011–2015. no. 270404. 1

[KBB*12] KOVNATSKY A., BRONSTEIN M. M., BRONSTEIN A. M., RAVIV D., KIMMEL R.: Affine-invariant photometric heat kernel signatures. In *Eurographics Workshop on 3D Object Retrieval* (2012), pp. 39–46. 3

[KBBK12] KOVNATSKY A., BRONSTEIN M. M., BRONSTEIN A. M., KIMMEL R.: Photometric heat kernel signatures. In *Scale Space and Variational Methods in Computer Vision* (2012), vol. 6667 of *LNCS*, pp. 616–627. 3

[KFR03] KAZHDAN M., FUNKHOUSER T., RUSINKIEWICZ S.: Rotation invariant spherical harmonic representation of 3d shape descriptors. In *Eurographics/ACM SIGGRAPH Symposium on Geometry Processing* (2003), Eurographics Association, pp. 156–164. 8

[KHK10] KANEZAKI A., HARADA T., KUNIYOSHI Y.: Partial matching of real textured 3d objects using color cubic higher-order local auto-correlation features. *Visual Comput. 26*, 10 (2010), 1269–1281. 2

[KMS00] KIMMEL R., MALLADI R., SOCHEN N.: Images as embedded maps and minimal surfaces: Movies, color, texture, and volumetric medical images. *Int. J. Comput. Vision 39*, 2 (2000), 111–129. 2

[KRB*13] KOVNATSKY A., RAVIV D., BRONSTEIN M. M., BRONSTEIN A. M., KIMMEL R.: Geometric and photometric data fusion in non-rigid shape analysis. *NM-TMA 6*, 1 (2013), 199–222. 3

[LJ05] LING H., JACOBS D.: Deformation invariant image matching. In *Computer Vision, IEEE International Conference on* (2005), vol. 2, pp. 1466–1473. 2

[Low04] LOWE D. G.: Distinctive image features from scale-invariant keypoints. *Int. J. Comput. Vision 60*, 2 (2004), 91–110. 3

[LZL*12] LIU Y.-J., ZHENG Y.-F., LV L., XUAN Y.-M., FU X.-L.: 3D model retrieval based on color + geometry signatures. *Visual Comput. 28*, 1 (2012), 75–86. 2

[NDL11] NIGGEMANN E., DE DECKER J., LÉVY M.: The New Renaissance, 2011. Report of the "Comité des Sages" Reflection group on bringing Europe's Cultural Heritage. 1

[OFCD02] OSADA R., FUNKHOUSER T., CHAZELLE B., DOBKIN D.: Shape distributions. *ACM T. Graphics 21*, 4 (2002), 807–832. 2, 3

[PP07] PAVAN M., PELILLO M.: Dominant sets and pairwise clustering. *IEEE T. Pattern. Anal. 29*, 1 (2007), 167 –172. 4

[PZC13] PASQUALOTTO G., ZANUTTIGH P., CORTELAZZO G. M.: Combining color and shape descriptors for 3D model retrieval. *Signal Process-Image 28*, 6 (2013), 608 – 623. 2

[RCMH09] RUIZ C., CABREDO R., MONTEVERDE L., HUANG Z.: Combining Shape and Color for Retrieval of 3D Models. In *INC, IMS and IDC, 2009. NCM '09. Fifth International Joint Conference on* (2009), pp. 1295–1300. 2

[SH07] STARCK J., HILTON A.: Correspondence labelling for wide-timeframe free-form surface matching. In *Computer Vision, IEEE International Conference on* (2007), pp. 1–8. 2

[Sin14] SINGH G.: CultLab3D: Digitizing Cultural Heritage. *IEEE Comput. Graph. 34*, 3 (2014), 4–5. 2

[Suz01] SUZUKI M.: A Web-based retrieval system for 3D polygonal models. In *IFSA World Congress and 20th NAFIPS International Conference. Joint 9th* (2001), vol. 4, pp. 2271–2276. 2

[TSDS11] TOMBARI F., SALTI S., DI STEFANO L.: A combined texture-shape descriptor for enhanced 3d feature matching. In *Image Processing, IEEE International Conference on* (2011), pp. 809–812. 2

[WCL*08] WU C., CLIPP B., LI X., FRAHM J.-M., POLLEFEYS M.: 3D model matching with Viewpoint-Invariant Patches (VIP). In *Computer Vision and Pattern Recognition, IEEE Conference on* (2008), pp. 1–8. 2

[Wei95] WEIBULL J.: *Evolutionary game theory*. MIT Press, Cambridge, Mass. [u.a.], 1995. 4

[ZBH12] ZAHARESCU A., BOYER E., HORAUD R.: Keypoints and local descriptors of scalar functions on 2D manifolds. *Int. J. Comput. Vision 100*, 1 (2012), 78–98. 3